Characterisation of the dynamics of organic contaminants (n -alkanes, PAHs and PCBs) in a coastal area

Agung Dhamar Syakti, Benjamin Oursel, Cédric Garnier, Pierre Doumenq

Characterisation of the dynamics of organic contaminants (*n*-alkanes, PAHs and PCBs) in a coastal area

Agung Dhamar Syakti [a,b,*], Benjamin Oursel [c,d], Cedric Garnier [d], Pierre Doumenq [e]

[a] Center for Maritime Biosciences Studies, Institute for Research and Community Service, Jenderal Soedirman University, Kampus Karangwangkal, Jl. dr. Suparno, Purwokerto 53123, Indonesia
[b] Marine Science and Fisheries Faculty, Raja Ali Haji Maritime University, Jl. Politeknik Senggarang-Tanjungpinang, Riau Islands Province 29100, Indonesia
[c] Institut Méditerranéen de Biodiversité et d'Ecologie marine et continentale (IMBE), Aix Marseille Université, CNRS, IRD, Avignon Université, 52 avenue Escadrille Normandie Niémen, 13013 Marseille, France
[d] Université de Toulon, PROTEE, EA 3819, 83957 La Garde, France
[e] Aix Marseille Univ, CNRS, LCE, Marseille, France

A B S T R A C T

The dynamics of three classes of organic contaminants, namely *n*-alkanes, polycyclic aromatic hydrocarbons and polychlorinated biphenyls, were evaluated from the settled suspended particulate matter (SPM) of two wastewater treatment plant outlets (O1 and O2) at the Marseille coast. We used a 1-m-high Plexiglas settling column filled with 7 L of seawater to determine the particles' settling rates, size distribution, and the extent of organic contaminants. Six classes of SPM (50–200 μm particles size) were obtained from 15 fractions of 500-mL successive filtering samples ranging from 30 s to 5 days, including those in the tube wall. The results of the experiment indicated that >68% of the particles settled within 15 min, which highly correlated with the distribution of organic carbon and contaminant contents. Furthermore, we demonstrated that 9%–13% of the SPM, which contained 5%–11% of the organic contaminants, are non-settable even after 5 days. Extrapolating such behaviour in situ using molecular diagnostic indices for organic contaminant source apportionment indicated that these non-settable contaminant particles are exported to the sea.

1. Introduction

Marseille is a large Mediterranean city that has been reinforced to gain an international reputation with the principal role as a Euro-Mediterranean trade centre. Such rapid urbanisation and industrialisation may have contributed to the pollution of the Mediterranean marine ecosystem. To mitigate any potential degradation in aquatic quality, a program known as EU Water Framework Directive was adopted in Europe to protect the discharge of pollutants and achieve a good ecological status of the surface and groundwater in 2015. The pollution load of the two main rivers of Marseille (i.e. Huveaune and Jarret) and the contributions of the wastewater system to the rivers provide a reflection of the activities upstream (in the watershed). Measuring 50 km in length and covering a watershed area of 523 km^2, the Huveaune River continuously drains the highly industrialised and urbanised valleys of Marseille and through normal flow or run-off episode transport. The Jarret River has a 102-km^2 catchment area along its 21 km of watershed and passes through forests, semi-natural habitats and agricultural land area (Oursel et al., 2014). The sewage system of the city of Marseille collects sewage and moves it toward the wastewater treatment plant (WWTP), which receives on average 250,000 m^3 of water per day and has a maximum capacity of 360,000 $m^3\ d^{-1}$. The WWTP has two outlet channels (O1 and O2), of which O1 is only active when the WWTP is bypassed (Fig. 1) because of an overflow caused by heavy rain. Because the runoff of both outlets carries sediments and related contaminants to the receiving marine waters in the centre of the newly established 'Calanque National Park' (established in 2012), the key question is whether such apportionment will have an adverse effect on the quality of the receiving water bodies and living organisms. The suspended particulate matter (SPM) in the rivers is one of the parameters affecting the water quality and contains a significant fraction of organic contaminants from the surrounding watershed (Lorrain et al., 2003; Vystavna et al., 2012). Organic contaminants in this study include, *n*-alkanes, polycyclic aromatic hydrocarbons (PAHs) and polychlorinated biphenyls (PCBs). Such organic compounds may have mutagenic and carcinogenic properties (Tian et al., 2013). Therefore, understanding the SPM transport behaviour is of special interest. Settling velocity is one of the essential parameters to investigate SPM transport behaviour (Perianez, 2005; Papenmeier et al., 2014), but measuring it directly in the river or other watershed forms is a difficult task because of changes in physicochemical properties, e.g., flocculation (Winterwerp, 2002;

* Corresponding author at: Center for Maritime Biosciences Studies, Institute for Research and Community Service, Jenderal Soedirman University, Kampus Karangwangkal, Jl. dr. Suparno, Purwokerto 53123, Indonesia.
E-mail address: agungsyakti@chemist.com (A.D. Syakti).

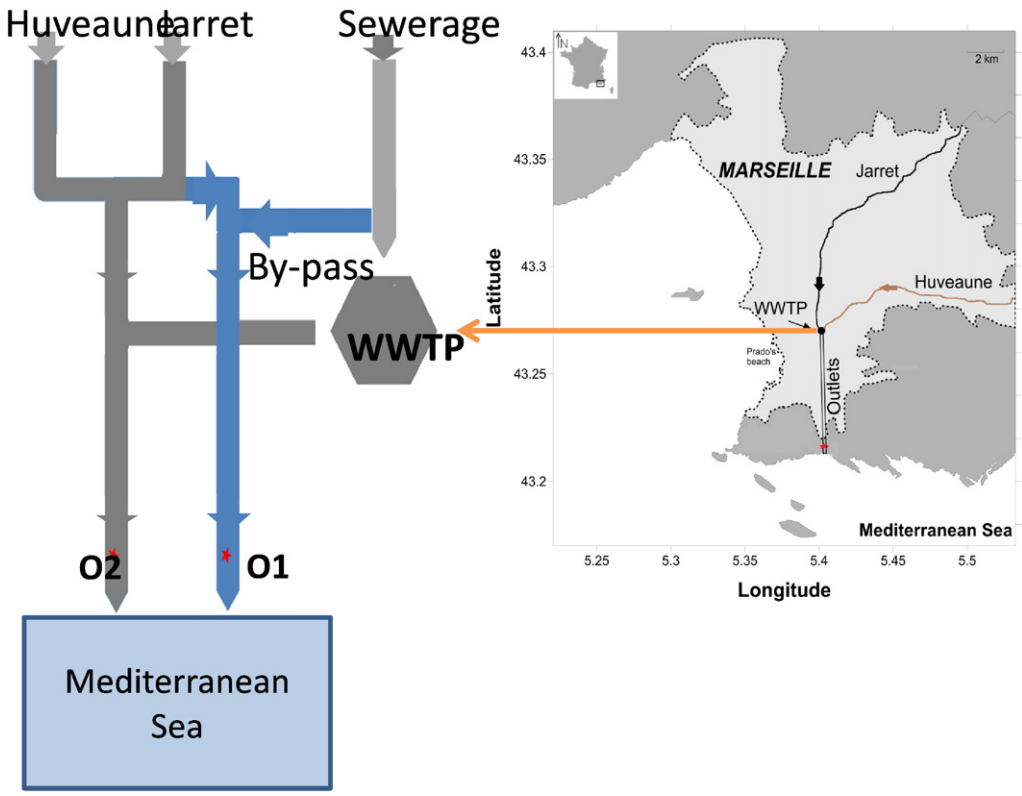

Fig. 1. Sampling site indicates the location of Emissaries 1 and 2 (O1 and O2), shown by a red star. The dotted area represents the urbanised zones of Marseille. Insert: schematic chart of O1 (only by-passed) and O2 point sources down streaming to the Mediterranean Sea.

Fugate and Chant, 2006). By using a simple device and experimental procedure, the present study aimed to investigate the settling velocity of the sediment particles and the distribution of the organic pollutants in different classes of the SPM matrix with regard to the dynamics of pollutants in a coastal environment.

2. Methodology

2.1. Origin of the settled particles

Sediment samples were obtained from the two outlets (O1 and O2) of the wastewater effluent canals. Both outlets relied on two main rivers that cross Marseille city, i.e. Huveaune and Jarret. O1 represents a location where the sample was collected during a heavy rain period. The settled SPM was constituted by the mixed waters of both rivers and the by-passed discharge from the WWTP (without treatment) because of the flood events.

In dry period (~300 days/year), the waters of both rivers go to O2 mixed with the treated WWTP effluent and are then channelled into the sea at the Calanque of Cortiou with a discharge of approximately 100 to 80,000 $m^3\ y^{-1}$.

2.2. Sampling and particle size distribution

Flood deposits were collected using a spatula and were placed in a bag, which was then placed in a cooler. Once in the laboratory, the samples were frozen at − 18 °C and were subsequently freeze-dried. The particle size distribution was determined using 50 g of these sedimentary particles, which were sieved for 20 min using a shaker table (Retsch AS200 control 'g') at an amplitude of 2 mm/'g'. The screens used were 2 mm, 1 mm, 500 μm, 200 μm, 63 μm and a receptacle. Before each use, the screens were cleaned and weighed, and finally, the mass percentage was calculated.

2.3. Settling rate experiment

A simple experimental device proposed by Oursel et al. (2014) was setup using two identical vertical Plexiglas tubes (1 m length and 10 cm diameter), open on the top and equipped with a valve at the bottom to collect water samples. The tube was filled with 7 L of coastal seawater sampled 2 km offshore and at a 4-m depth and then acclimatised for 1 day to obtain a homogeneous temperature of the water column (close to 20 °C). During this time, 7 g of dried particles (flood deposit sediments) were weighed, placed in a 50-mL syringe, and wetted with few mL of milliQ water (Millipore 18.2 MΩ). Considering the seawater volume, a final SPM average concentration of 1 g L^{-1} was reached, which corresponded to the same range of SPM recorded in the rivers and outlet during flood events (data not shown); this led to a sufficient particle mass for subsequent chemical analysis. After 1 day of wetting, the particles were injected on the top of the system. To cover a large domain of settling particles and sizes, the Plexiglas tube's water content was divided into 14 sub-samples (fractions; $f1$–$f14$) of 500 mL each withdrawn from the bottom of the tube after 30 s; 2, 5, 10, 20, 40 and 70 min; 2, 3, 4, 8 and 24 h; and 5 days and the remaining liquid fraction in the bottom space of the Plexiglas column. Plexiglas is a material known to induce electrostatic attraction, which might prevent very light particles to settle; therefore, the last (15th) fraction ($f15$), which had remained inside the tube, may be hypothesised as the fraction that can be directly exported to the open sea. For further analysis, we grouped the fractions (f) into six classes: $f1 + f2$ = A; $f3$ = B; $f4$ = C; $f5$–$f7$ = D; $f8$–$f14$ = E; $f15$ = F. For illustration, sample number O1A represents a sample from O1 and fractionated from sub-sample $f1$ and $f2$, which were collected from the bottom of the tube after 30 s and 2 min, then grouped as class fraction A.

The average velocity of the settling particles (w_s; in m s^{-1}) of each fraction was governed by Stokes' law (Mantovanelli and Ridd, 2006), and the particle diameter (Ø; in m) for a given settling velocity was

calculated according to Oursel et al. (2014) for diameters varying from >276 to <0.78 μm. Prior to the analysis, a small portion (10%) of the collected samples was filtered through 25-mm glass filters (Whatman GFF, 0.7 μm) for particulate organic carbon (POC) analysis. The remaining water was later filtered through 47-mm glass filters (Whatman GFF, 0.7 μm) for organic contaminant (hydrocarbons and PCBs) identification and quantification. All GFF filters were pre-calcinated for 4 h at 450 °C.

2.4. Particulate organic carbon

Total carbon contents were quantified from the sediments using a TOC-V_{CSH} analyser (Shimadzu) coupled with an SSM-5000A module. The total and organic carbon contents were determined using a high-temperature (900 °C) catalytic oxidation method with CO_2 IR detection (Ammann et al., 2000, Callahan et al., 2004), calibrated using glucose (Analytical reagent grade, Fisher Scientific), with an accuracy of 0.1 mg C. For POC analysis, GFF filters were dried to a constant weight at 60 °C and then exposed to HCl fumes for 4 h to remove all the inorganic carbon (Lorrain et al., 2003).

The particulate inorganic carbon contents were quantified from the sediments using the same analytical equipment as above after the addition of H_3PO_4 (analytical reagent grade 85%, Fisher Scientific) at 200 °C followed by CO_2 IR detection, calibrated using $NaHCO_3/Na_2CO_3$ (Shimadzu), with an accuracy of 0.1 mg C. Then, the POC content was calculated as the difference between the total and inorganic carbon contents.

2.5. Organic contaminant extraction and separation

Hydrocarbons and PCBs were extracted from the glass filter samples (classes) into a clean cellulose extraction thimble using a Soxtherm apparatus. The extraction procedure was performed according to Syakti et al. (2012). The aliphatic hydrocarbons and PCBs (F_1) and aromatic (F_2) fractions were separated using a 1.0 × 30-cm borosilicate glass column with 8 g of silica gel and 8 g of alumina (at the bottom and top of the column, respectively). Before use, both adsorbents were deactivated with 5% (w:w) distilled H_2O. F_1 was eluted with 30 mL of HEPT and 20 mL of HEPT/DCM (90:10, v:v). A 40-mL HEPT/DCM (80:20, v:v) elution yielded F_2. Both fractions were evaporated before analysis. The resulting sum ($F_1 + F_2$) provided the total hydrocarbon content. Sulphur interference was removed by shaking the extract with Cu powder that had been washed with dilute HCl (1:4, v:v).

2.6. Gas chromatography-mass spectrometry analysis

The fractionated extracts were analysed for resolved alkanes, PCBs (F_1) and PAHs (F_2) by capillary gas chromatography coupled to mass spectrometry (GC–MS; Autosystem XL GC and TurboMass from Perkin Elmer, USA), with data reported as $\mu g \cdot kg^{-1}$ dry weight (dw). The chromatographic conditions were as follows: splitless injection (30 s), Elite 5MS column (30 m × 0.25 mm i.d. × 0.25 μm film thickness, Perkin Elmer). The PSS injector was programmed from 50 °C (0.1 min isothermal) to 250 °C (200 °C·min^{-1}) to minimise the solvent peak. For F_1 and F_2, the GC oven was temperature-programmed from 40 °C (2 min isothermal) to 120 °C (45 °C·min^{-1}) to 310 °C (5 °C·min^{-1}) and held isothermally for 20 min. For the PCBs, the oven was programmed from 100 °C (3 min isothermal) to 290 °C (6 °C·min^{-1}) (10 min isothermal). The mass spectrometer was operated in positive electron impact ionisation mode (70 eV) and simultaneously scanned in both full scan and selected ion monitoring mode. Individual *n*-alkanes were quantified using [$^2H_{40}$]*n*-nonadecane as surrogate and 1-eicosene as internal standard. For PAH analysis, the 16 US EPA priority PAHs were identified from their retention time and *m/z* ratios and then were quantified using surrogates [$^2H_{10}$]phenanthrene *m/z* 188 and [$^2H_{12}$]chrysene *m/z* 240] and internal standard ([$^2H_{10}$]pyrene). The seven PCBs and pesticides were quantified with Mirex (*m/z* 235–274) as surrogate. The abbreviations, common names and diagnostic ions for the PAHs were as follows: Na, naphthalene (*m/z* 128); Ac, acenaphthylene (*m/z* 152); Ace, acenaphthene (*m/z* 153); Fr, fluorene (*m/z* 166); Phen, phenanthrene (*m/z* 178); Ant, anthracene (*m/z* 178); Fl, fluoranthene (*m/z* 202); Pyr, pyrene (*m/z* 202); Chry, chrysene (*m/z* 228); B[*a*]A, benzo[*a*]anthracene (*m/z* 228); B[*a*]Pyr, benza[*a*]pyrene (*m/z* 252); B[*e*]Pyr, benzo[*e*]pyrene (*m/z* 252); B[*b*]Fl, benzo[*b*]fluoranthene (*m/z* 252); B[*k*]Fl, benzo[*k*]fluoranthene (*m/z* 252); B[*ghi*]P, benzo[*ghi*]perylene (*m/z* 276); IPyr, indeno[1,2,3-*cd*]pyrene (*m/z* 276); and dB[*a*, *h*]Ant, dibenzo[*a*, *h*]anthracene (*m/z* 278).

2.7. Quality control and quality assurance

All analytical data were subject to quality control procedures. All content data are provided on a dw basis. Procedural blanks were run between each batch of four samples, and no contamination was found. The reproducibility estimated for triplicate samples was >92%. A standard reference material (Harbour Marine Sediment HS-5) (LGC Promochem) was analysed to evaluate the extraction accuracy (95 ± 7%). The mass of each individual PAH in the blanks was insignificant relative to that in the samples. The detection limits for *n*-alkanes and PAHs were determined as the content generating a peak with a signal/noise ratio of 3. The detection limits for *n*-alkanes and PAHs in the real samples were 0.2 and 2 $\mu g \cdot kg^{-1}$ dw, respectively, and it was 0.5 $\mu g \cdot kg^{-1}$ dw for the PCBs.

2.8. Principal component analysis

Data analysis included calculating individual and total *n*-alkane, PAH and PCB concentrations and the use of a molecular diagnostic ratio and principal component analysis (PCA). The PCA was limited to a cluster dendogram of the pollutants and eigenvector plots for the SPM deposit class analysis reflecting the affinity in their behaviour in relation to the sediment settling experiment. These factors were row-combined into a single matrix *X* to determine the main directions of the observation space along which the data have the highest variability, and the eigenvalue decompositions of the variance matrix were calculated with the centred matrix to denote their matrix transposition. All *n*-alkanes (*n*-C_{12} to *n*-C_{38}) in the sediments, including pristane (Pr) and phytane (Phy), PAHs and PCBs, were subjected to PCA. In this work, the PCA with two components was then performed on this data subset. R 2.12.2 and RStudio 0.93.92 software from GNU R, Boston, USA, were used for the PCA.

3. Results and discussion

3.1. Settling velocities and organic matter contents

The settling velocities of the flood deposits from O1 and O2 were calculated according to Mantovanelli and Ridd (2006). That is, the water column length (H_{wc}; in m), and the corresponding sedimentation time (t_s; in s) were used to calculate the settling velocity (w_s; in m s^{-1}), as shown in Eq. (1):

$$w_s = \frac{H_{wc}}{t_s} \quad (1)$$

Moreover, as w_s is already known, the diameter of the particle can be predicted through the following equations, which are governed by Stoke's law (Eq. (2)):

$$w_s = \frac{2 \times g \times (\rho_s - \rho_w)}{9\mu} \times r^2 \quad (2)$$

where g is the gravitational acceleration (in m s^{-2}), ρ_s and ρ_w are the solid and water densities, respectively, μ the fluid's dynamic viscosity

Table 1
Settling velocities and diameter estimation of deposit flooding particles from wastewater treatment emissaries (O1 and O2).

Filter fraction	Withdrawal time and condition	Class fraction	Velocity (μm s^{-1})	Calculated diameter (μm)	Mass distribution dw (mg)		TOC (mg/g)	
					O1	O2	O1	O2
1	30 s	A	64,285.7	276.6	1636	380	220	160
2	2 min	A	12,142.9	120.2	1721	2807	236	103
3	5 min	B	4081.6	69.7	1522	1930	225	102
4	10 min	C	1785.7	46.1	690	671	112	102
5	20 min	D	823.4	31.3	379	343	250	118
6	40 min	D	374.5	21.1	381	187	231	121
7	70 min	D	186.3	14.9	174	85	232	120
8	2 h	E	96.9	10.7	86	81	236	129
9	3 h	E	55.4	8.1	61	50	242	118
10	4 h	E	36.1	6.6	44	30	206	123
11	8 h	E	16.3	4.4	31	18	149	88
12	24 h	E	4.1	2.2	40	54	60	37
13	5 days	E	0.5	0.8	12	10	47	104
14	Remaining liquid	E	0.1	0.1	11	20	76	84
15	Washed inner wall	F	0.05	0.05	744	1218	211	107

(in kg m^{-1} s^{-1}) and r the equivalent particle radius (in m). As the exact solid density of the particles was unknown, the solid density of quartz was used as a reference ($\rho_s = 2650$ kg m^{-3}). The fluid's dynamic viscosity was calculated for seawater after temperature correction (e.g., 1.07×10^{-3} kg m^{-1} s^{-1} at 20 °C).

Table 1 shows that the amount of bulk particles were higher in classes A, B, C and F than in D and E classes. The median particle size (D50) for both the flooding deposits was 10.7 μm, with an average of approximately 41 μm. The particle size settling velocity estimates ranged from approximately 0.05 μm s^{-1} to 64 mm s^{-1}, with a median settling velocity of 97 μm s^{-1}. Geyer et al. (2004) had reported that the settling velocity value for aggregates of fine material was approximately 1 mm s^{-1}. Therefore, class D, E and F are potentially transported without a risk of particle aggregation and flocculation. In nearly all samples, the POC contents were within the same greater magnitude: on average, 147 ± 60 and 85 ± 23 mg/g for O1 and O2, respectively. These results suggest a good correlation between the organic matter content and particle sizes of 2–45 μm. The four fastest sinking classes (A–C; <10 min of settling) represented approximately 31% and 47% of POC for O1 and O2, respectively, and class D (20 to 70 min) represented approximately 25% and 33% of POC, respectively. The slower sinking classes, E (2 to 60 h) represented approximately 36% and only 3% of the POC in O1 and O2, respectively. The remaining classes were approximately 8% and 17% of the POC, the particles of which were potentially distributed for a long distance toward the sea for O1 and O2, respectively. Previously, who used surface sediments from Rhone River, demonstrated that larger particles (>125 μm; 80% of the bulk particles estimated) settled faster than finer particles (<63 μm), which remained in the suspension phase and further settled at a longer distance from their sources.

3.2. Contaminant behaviour

The average POC content was determined for the six classes of settled sediment (A–F) (Table 1). We observed pollutant behaviour between two channel outlets (O1 and O2). In many cases, O1 contained more concentrated contaminants than O2. Because Marseille has a non-separated sewage network that collects both wastewater and run-off, O1 is only active when the WWTP is by-passed because of the limited capacity of the WWTP in heavy rain; therefore, the flood deposit is likely to contain non-treated sewage particles. For instance, ∑PAHs and ∑PCBs were higher in all classes of O1. Conversely, the *n*-alkanes in O1 were observed at a lesser extent in classes A, C and E than in classes B, D and F. Assuming that the particles will be settled in the marine environment after 5 days of

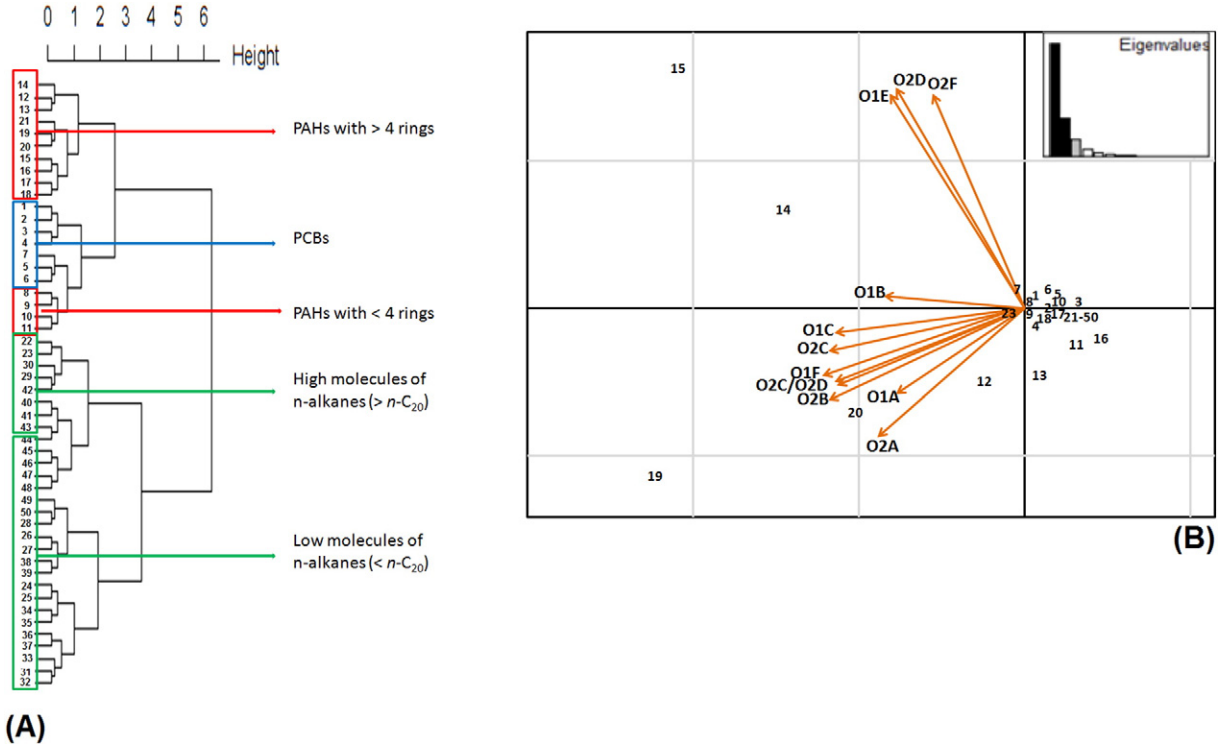

Fig. 2. Cluster dendogram (A) of the pollutants and Eigenvector plots (B) for SPM deposit classes analysis (A-F: O1A-E2F) reflecting affinity in their behaviour in relation with sediment settling experiment. 1 (CB-28), 2 (CB-52), 3 (CB-101), 4 (CB-118), 5 (CB-138), 6 (CB-158), 7 (CB-180), 8 (Na), 9 (Ace), 10 (Ac), 11 (F), 12 (Phen), 13 (Ant), 14 (Fl), 15 (Pyr), 16 (B[*a*]A), 17 (Chry), 18 (B[*b*]Fl), 19 (B[*k*]Fl), 20 (B[*a*]Pyr), 21 (IPyr), 22 (dB[*a,h*]Ant), 23 (B[*ghi*]P), 24 (n-C_{14}), 25 (n-C_{15}), 26 (n-C_{16}), 27 (n-C_{17}), 28 (Pr), 29 (n-C_{18}), 30 (Phy), 31 (n-C_{19}), 32 (n-C_{20}), 33 (n-C_{21}), 34 (n-C_{22}), 35 (n-C_{23}), 36 (n-C_{24}), 37 (n-C_{25}), 38 (n-C_{26}), 39 (n-C_{27}), 40 (n-C_{28}), 41 (n-C_{29}), 42 (n-C_{30}), 43 (n-C_{31}), 44 (n-C_{32}), 45 (n-C_{33}), 46 (n-C_{34}), 47 (n-C_{35}), 48 (n-C_{36}), 49 (n-C_{37}), 50 (n-C_{38}).

transport from the river shed and WWTP, 5.5%–12%, 2%–17% and 15% of *n*-alkane, PAH and PCB loadings, respectively, will enter the marine ecosystem. In this study, the O1 sample was obtained during a flood period (Meteofrance) that showed 609 mm y^{-1} of rain on average. Oursel et al. (2014) have evaluated the annual global SPM discharge to be approximately 3950 t, with 850 t coming from rivers, highlighting the main contribution of the TWW in such conditions. The O2 sample corresponds to the sampling period in which there was only 30 mm of cumulative rainfall (Meteofrance), which represents approximately 2% and 12% of the month's total water and SPM discharge, respectively.

Fig. 2 shows the dendogram analysis for all pollutants using PCA. We found that the pollutants can be grouped into four main clusters, i.e., *n*-alkanes and PAHs combined with PCBs. The distribution of *n*-alkanes is markedly divided into two sub-groups that represent both low- and high-molecular-weight *n*-alkanes; however, as seen in Fig. 3, the alkanes were not affected by the variation of the classes of deposit sediments. In contrast, high-molecular-weight PAHs (>4 benzene rings) seem to be affected by the classes B (~70 μm) and E (0.1–10 μm) for O1 and D (15–30 μm) and F (0.05 μm) for O2. Low-molecular-weight PAHs (<4 rings) showed similar behaviour with the PCBs, which are

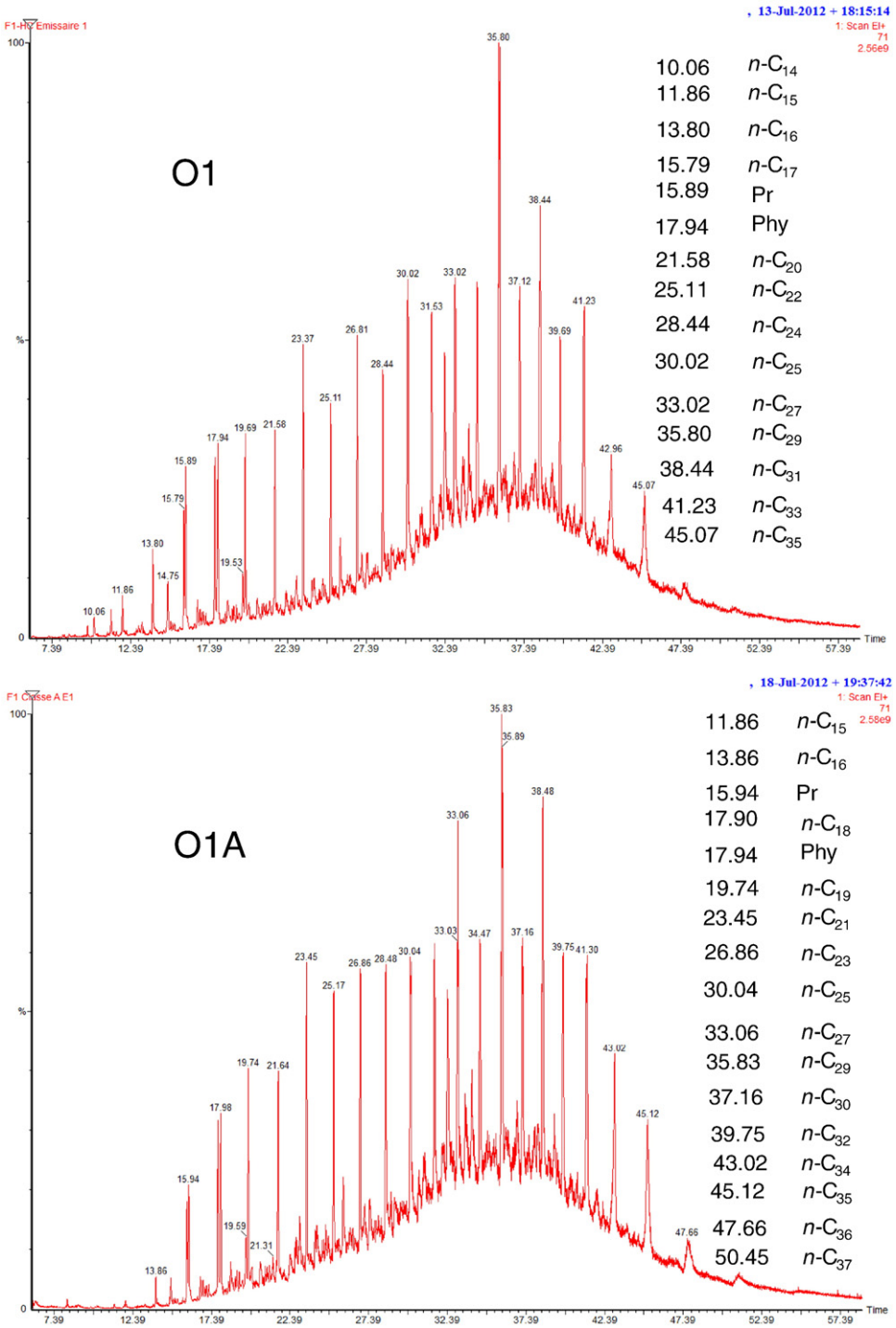

Fig. 3. Capillary column gas chromatograms of the saturated hydrocarbons fractions of bulk particle from emissary 1 (O1) and examples of class fraction of sediment experimentation (O1A, O1B and O1E).

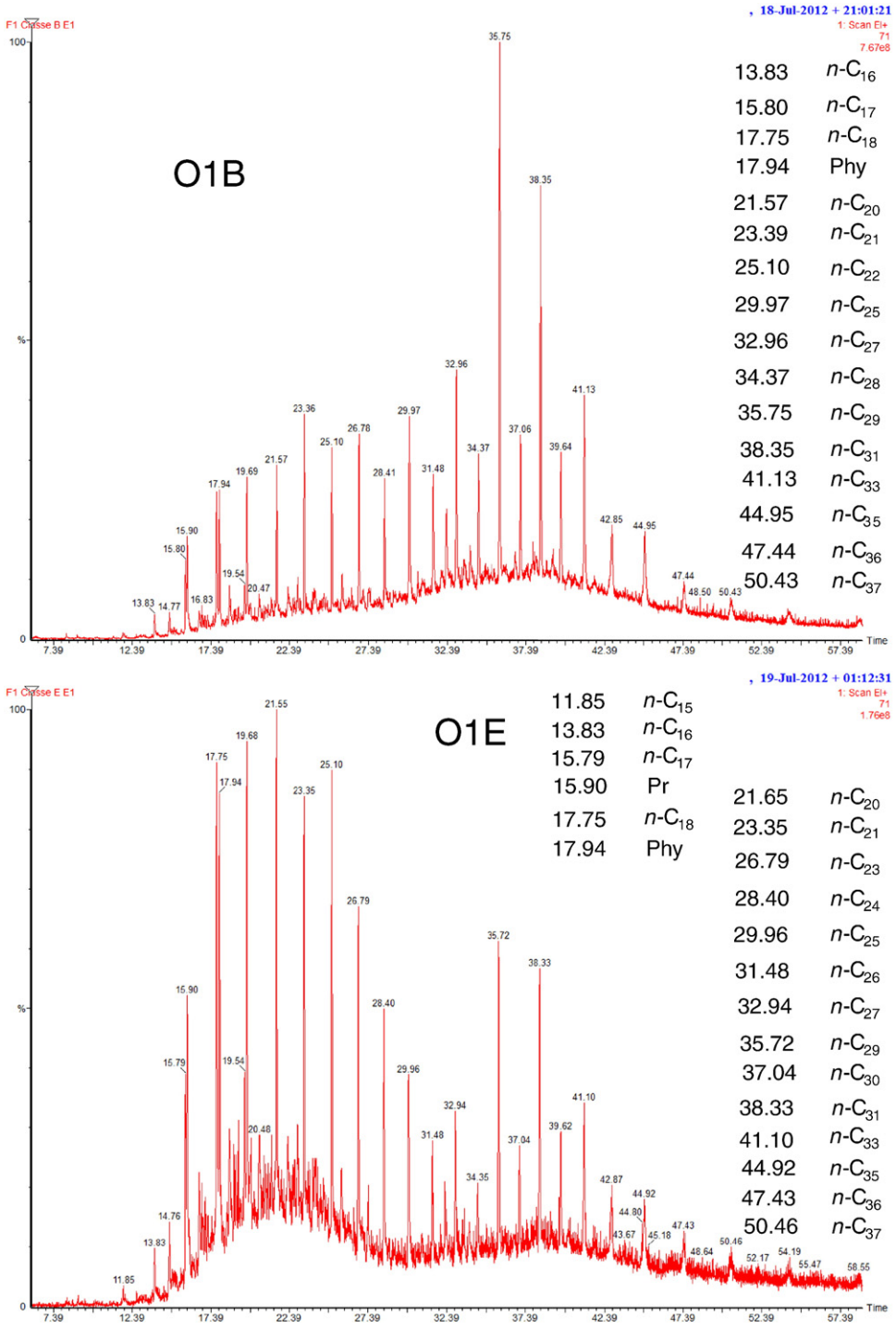

Fig. 3 (*continued*).

distributed with the same proportion within classes A, C, D and F for O1 and classes A, C, D and E for O2.

3.2.1. n-Alkanes

The understanding of the distribution of *n*-alkanes with regard to settling velocities needs to be reinforced through the use of GC patterns of aliphatic hydrocarbons and some diagnostic indices previously applied in the environmental chemistry field. Fig. 2 shows that the *n*-alkane profile of both bulk O1 and O2 seem to be apportioned as reported by Huveaune and Jarret. $\sum n$-alkanes OC varied greatly among the five class fractions (Fig. 3 and Table 2). The larger size fraction (A and B; >63 μm) had higher *n*-alkane concentrations in both O1 and O2 sediments, ranging from 48 to 246.5 (ng/g OC dw). In terms of the correlation between *n*-alkane concentration and TOC, this study revealed a correlation with $r^2 = 0.7$. Contrary to our finding, Jeng and Chen (1995) found no grain size effect for the *n*-alkanes and *n*-fatty acids, but the ratios of branched-chain to normal fatty acids increased progressively with decreasing particle size and correlated highly with bound organic carbon, suggesting an increasing input of intact bacterial phospholipids(Mazzella et al., 2007).

For O1, we suggest that the largest class fraction (A) contains more *n*-alkanes with >20 carbons and such high-molecular-weight

Table 2
$\sum$ *n*-alkanes, $\sum$ PAH and $\sum$ PCB concentrations, sediment characteristics for deposit settling particles from wastewater treatment emissaries (O1 and O2). Bulk O1 and O2 contains 659.6 and 587.3 of $\sum$ *n*-alkanes OC (ng/g OC dw), respectively.

Classes	Mass contribution to total sediment dw (%)		TOC (%)		$\sum$ *n*-alkane OC (ng/g OC dw)		$\sum$ PAH OC (ng/g OC dw)		$\sum$ PCB OC (ng/g OC dw)	
	O1	O2	O1	O2	O1	O2	O1	O2	O1	O2
A	44.6	40.4	18.5	17.4	128.5	246.5	357.6	546.7	53.5	28.4
B	20.2	24.5	8.2	6.8	95.8	48.0	538.6	496.3	17.0	15.9
C	9.2	8.5	4.1	6.3	9.3	43.7	656.0	260.1	–	–
D	12.4	7.8	25.2	21.6	65.2	35.2	372.7	25.2	87.2	21.5
E	3.8	3.3	36.1	41.6	24.0	38.1	20.4	18.6	14.4	–
F	9.9	15.4	7.9	6.2	42.2	23.8	356.2	30.1	16.5	–
Total	100	100	100	100	353	435.3	2308.2	1377.0	110.6	46.8

compounds (HMW, >20 carbon atoms) decreased gradually with the decrease in the size of particles (Class B > C > D > E). A slight increase in HMW in class F was obviously due to mixed remaining particles attached in the inner wall of the tube. As HMW *n*-alkanes at *n*-C_{29} or *n*-C_{31} are commonly used as indicators for terrestrial input because of their presence in prominent higher plant input (Kanzari et al., 2014), this study revealed the fate of terrestrial input seaward in relation to particle size (Fig. 3–4, Table 3). Our study is in agreement with another study conducted by Wang et al. (2010) and de Souza et al. (2011), which confirmed a good correlation between the concentration of C_{25}–C_{31} *n*-alkanes and TOC in the sediments of river basins (r2 > 0.8).

Markedly observed in O2, the influence of the WWTP can be observed with bimodal unresolved complex mixture (UCM), indicating a possible weathering process in the WWTP or simply tracer markers of the bulk sediment of the Jaret River.

The ratios *n*-C_{17}/Pr and *n*-C_{18}/Ph were measured for all flooding classes. The comparison between O1 and O2 showed that these values were slightly different. The whole value was below 1, which indicates apportionment from non-treated organic compounds, e.g., petroleum hydrocarbons. The first class fraction (>100 μm of particle size), which represents >40% of the organic mass contribution, was responsible for this value. A predominance of odd numbered *n*-alkanes (*n*-C_{27}, *n*-C_{29} and *n*-C_{31}) were found in all other classes, which is an evidence of important and recent terrigenous inputs entering the Cortiou channel through the Houvenau and Jarret rivers. The terrigenous/aquatic ratio (TAR) (Bourbonniere and Meyers, 1996; Mille et al., 2007), derived from a ratio between the concentrations of long-chain *n*-alkanes ($nC_{27} + nC_{29} + nC_{31}$) to short-chain *n*-alkanes ($nC_{15} + nC_{17} + nC_{19}$), revealed the importance of terrigenous inputs vs. aquatic inputs. This ratio is very high for all class fractions, except for the class O2E.

Interestingly, if we focus on class fraction E (0.1–10 μm), for both O1 and O2 (Table 5), the distribution of *n*-alkanes shows a predominance of the even carbon number preference of the C_{14}–C_{20} *n*-alkanes, and it has been cautiously suggested that the molecular signatures of these *n*-alkanes are known to originate from marine bacteria (Grimalt and Albaiges, 1987, Syakti et al., 2012).

The latter raised a question of whether the ratio of the particle size affects the distribution of *n*-alkanes. We further tested a ratio newly proposed by Syakti et al. (2012), Terrestrial Marine Discriminant (TMD) index. Through this index, we found the SPM class fraction E (O1E and O2E) may be responsible for the non-terrestrial molecular signatures found in the marine sediment environment.

3.2.2. PAHs

Thirteen compounds from 16 PAHs listed by the EPA have been detected and quantified from the O1 and O2 flooding deposit experiment. Comparing the two experiments, the results showed the distribution of individual PAHs was within a similar distribution of greater amplitude where the $\sum$ PAH concentrations for O1 and O2 in the bulk sediment were 4075 and 3779 $\mu g \cdot kg^{-1}$ dw, respectively. Because of the variability in complex sediments, when all the class fractions were added (A–F), we noted the loss of some compounds, ca. 10% and 40%, respectively, for O1 and O2. Our results might be due to the fate of various PAHs, which vary widely even though they generally have a strong physicochemical family resemblance. For example, we found only Ac, B[*a*]Ant and dB[*ah*]Ant in the O1 and O2 total bulk, and they were completely absent in most of the class fractions. It is known that with a Henry's Law constant of 1.13×10^{-5} atm-cu m/mol at 25 °C, the volatilisation of acenaphthylene from the environment is suggested to be important. Another example is the Ant with three times the magnitude in O1 compared to that in O2. Such a compound will strongly adsorb to the sediment and particulate matter, but in O2 from which the water was supposed to be treated resulting in compound hydrolysis and photolysis near the surface of the WWTP treatment units (Zhang et al., 2012). O1, however, contains 2–5 times more Ac, Fr, Phe, Ant, and Indino compounds than O2. These results might be related to the fact the O1 was by-passed when there was heavy rain, leading to non-treated wastewater and storm water from Marseille city (Fig. 2 and Table 4.).

Discussing each individual PAH compound's behaviour may be excessive; therefore, a simple relative ratio of each individual PAH versus the $\sum$ PAHs was used to better understand the pollutant behaviour within each class fraction. By using such an approach (Fig. 4A and B), we can focus on four compounds that have consistent behaviour. For instance, pyrene was the compound with the highest concentration for both O1 and O2 in class fraction E (<15 μm). As class E consisted of the sediment particles that can sediment in >2 h up to 5 days, we can expect its concentration will be higher seaward. This high molecular PAH was 46.4% to 46.8% of the total bulk quantified PAHs. The occurrence of pyrene has been reported in the estuary and marine sediments, including hydrothermal vents (Zhou et al., 1998; Geptner et al., 2006; León et al., 2014). In this class fraction, after pyrene, fluoranthene and fluorene were the compounds that have a relatively high percentage consistently both in the O1 and O2 class fraction E (<15 μm). Another PAH, i.e., B[*k*]Fl was found with the average percentage of approximately 23% for both O1 and O2 (Fig. 5). In fact, F, Fl, Pyr and B(k)F with their high Kow and Koc values (ranging from 4.7–6.8) can be strongly associated with particulate matter and rapidly absorbed onto sediments, where they are stable for decades or more (Patrolecco et al., 2010; Birch et al., 2012). The Eigenvector profile for this compound was markedly shown in the extremity of the plot (Fig. 2). The low solubility and high affinity with organic matter of these PAHs tend to be associated with high levels of organic carbon. Surprisingly, in this study, compounds were found in the classes with a high percentage of small particles, i.e., <63 μm. Additionally, several authors (Neşer et al., 2012; Commendatore et al., 2012) reported that subtidal sediments correspond with sediments that shows particle similarity with class fraction D and/or E, which in the end favoured the accumulation of HMW due to their increased particle sorption affinity and resistance to degradation.

Moreover, to describe PAHs' characteristics in relation with settling velocity classes, we used four diagnostic compound ratios that are widely used to differentiate PAH sources (Yunker et al., 2002; Commendatore et al., 2012) (Table 4). For instance, Ant / (Ant + Phe)

is widely used to differentiate between sources of combustion and oil. The threshold boundaries proposed by Yunker et al. (2002) are defined as 0.1 and 0.4, and the values below these thresholds would be of petroleum rather than combustion/pyrolytic transition origin. Using these indices, we determined that the entire classes of both O1 and O2 were of biogenic combustion origin. However, the total bulk of O2 showed a ratio of Ant / (Ant + Phe) below 0.1, indicating petroleum origin. Moreover, the ratio Fl / (Fl + Pyr) ranged from 0.5–4.9, which also supported the theory of mixed biogenic and petrogenic combustion/pyrolytic source. Concerning IPry / (IPyr + B[*ghi*]P), their value ranged from 0.4–0.8. According to Hartmann et al. (2004), these values indicated wood and coal combustion. Previous works in this area conducted by Sanderson et al. (2004) and Kanzari et al. (2012) showed that the atmospheric transport of PAHs from highly urbanised areas (traffic of trucks and cars) is the most probable pyrogenic sources of the PAHs. The last ratio, LMW/HMW (sum of two- and three-ring PAHs to the sum of more than three-ring PAHs) ratios (<1) often indicate PAHs that are derived mainly from pyrogenic sources (Wang et al., 2006; Table 4). Similar to what we discussed earlier (*n*-alkanes), PAHs ratios may give conflicting results for assessing sediments apportionment when the environmental matrixes were analysed without further fractionation. Such phenomena may be caused by low content and mixed-source organic matter. This finding might raise a question of the importance of particle size for such an organic geochemistry application.

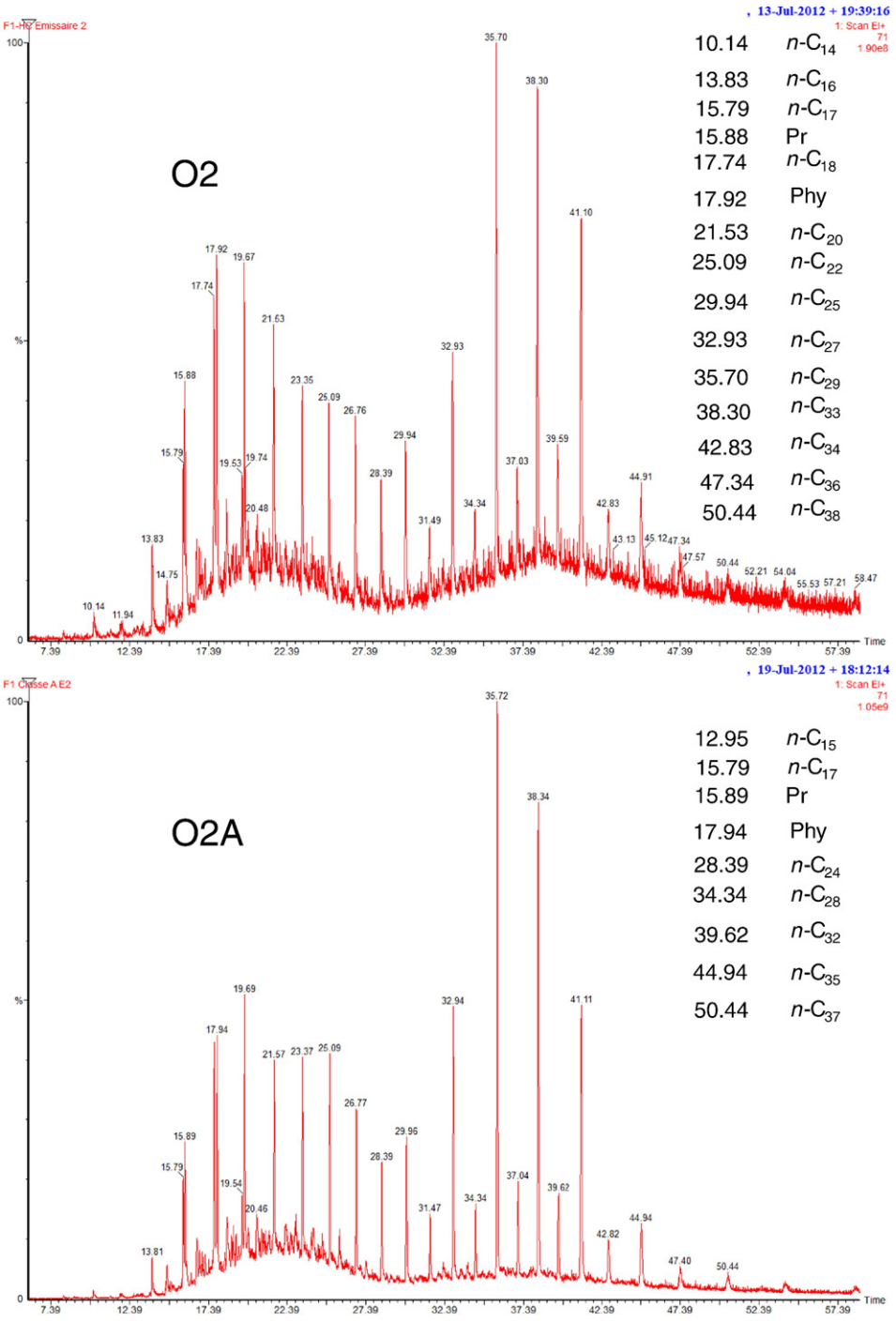

Fig. 4. Capillary column gas chromatograms of the saturated hydrocarbons fractions of bulk particle from emissary 2 (O2) and examples of class fraction of sediment experimentation (O2A, O2B and O2E).

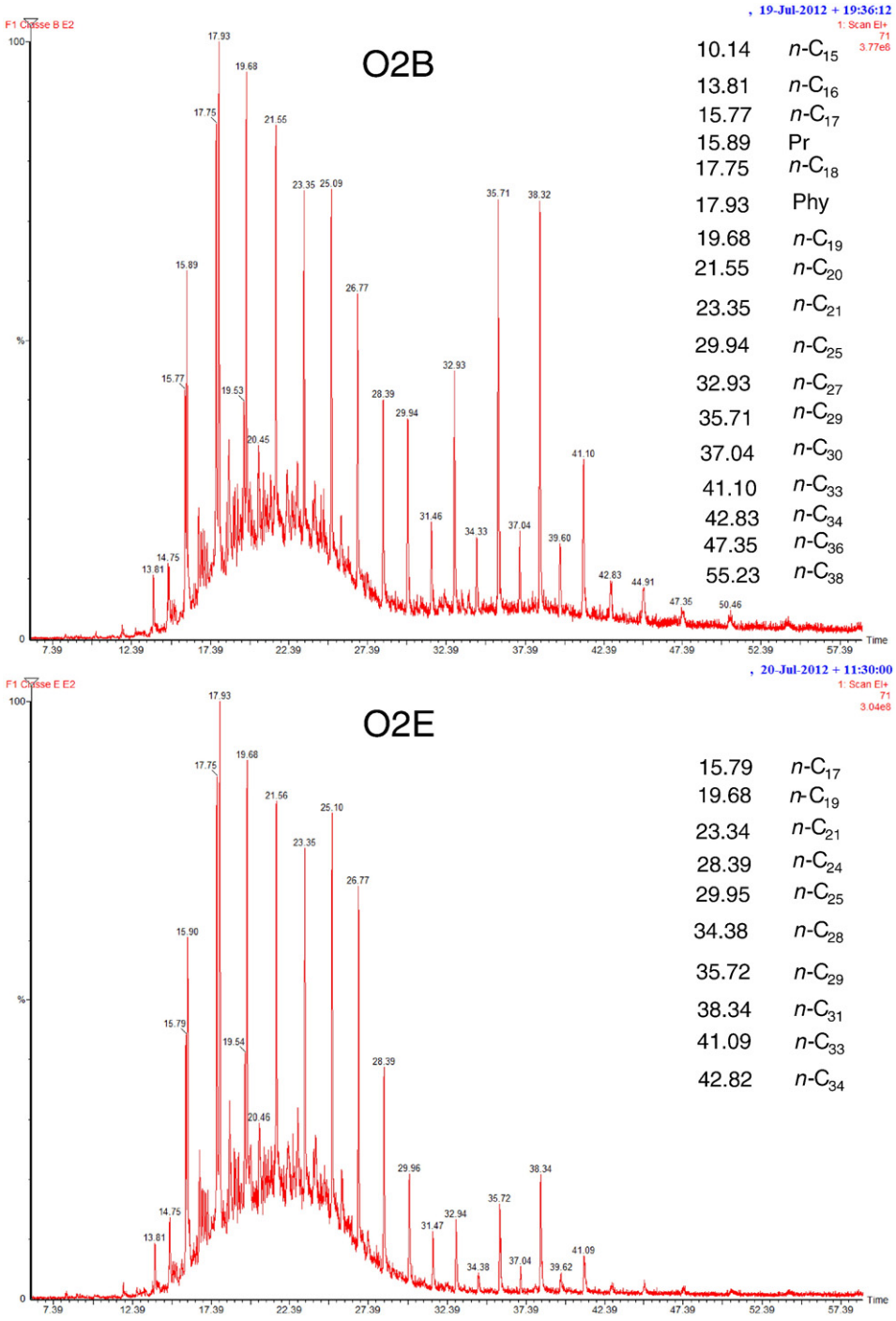

Fig. 4 (*continued*).

3.2.3. PCBs

Our results showed 5 of 7 PCBs ICES have been detected in both SPM deposits from O1 and O2. On average, CB-101, CB-118, CB-138, CB-153, and CB-180 contribute 17%, 29%, 30%, 20% and 5% of the total ICES, respectively. Relatively high concentrations of PCBs were measured in O1, ca. three fold of that in O2. This observation reinforces our finding related to the non-treated water from O1 due to flooding events. The dominating PCB congeners in both O1 and O2 were CB-118 (penta-chlorinated) followed by CB-138 (hexa-chlorinated). The congener pattern was not consistent throughout the classes, although it appeared that CB-101 was highly distributed in all O1 classes, while it was absent in the O2 for C–F classes. Previous studies conducted by Jany et al. (2012) showed slightly different patterns, demonstrating that CB-153, CB-180 and CB-138 were the individual congeners with highest PCB content, respectively. The absence of CB-28 and CB-52 can be explained by the fact that the congeners with 2–3 chlorine atoms and selected bio-degradation profile are less prominent in commercial mixtures of PCBs compared to those tetra-, penta-, hexa- and heptachloro biphenyls. Despite being banned in 1980 because of their widespread use in transformers, electrical equipment and other industries in several countries (Barakat et al., 2002), previous studies have reported their presence in the environment, i.e., in the Marseille coast (Wafo et al., 2006; Syakti et al., 2012). Fig. 2 clearly shows PCBs' settling distribution, which is similar to PAHs' behaviour, in particular, those containing a low number

Table 3
Concentration of *n*-alkanes in sediment samples of emissary 1 and 2 (O1 and O2) and their respective class fractions (μg·kg^{-1} dw).

n-Alkane	O1	O2	O1A	O1B	O1C	O1D	O1E	O1F	O2A	O2B	O2C	O2D	O2E	O2F
n-C_{14}	2.2	3.2	0.1	<0.1	<0.1	0.1	<0.1	<0.1	<0.1	0.5	0.1	nd	nd	nd
n-C_{15}	4.1	1.0	0.1	0.1	0.1	<0.1	0.2	<0.1	<0.1	0.2	0.1	<0.1	<0.1	<0.1
n-C_{16}	7.6	12.3	0.6	0.6	0.1	0.3	0.3	0.2	0.6	2.3	0.5	0.3	0.4	0.3
n-C_{17}	9.1	13.8	1.1	1.5	0.2	1.2	0.8	0.9	1.5	5.5	1.4	1.3	1.7	1.0
Pr[a]	11.8	31.0	1.5	22	0.3	1.8	1.6	1.6	2.9	7.8	2.9	2.4	3.0	2.0
n-C_{18}	14.9	25.0	2.5	2.6	0.3	2.1	1.4	1.4	2.9	9.3	2.7	2.3	2.8	2.0
Phy[b]	16.2	29.6	2.8	2.8	0.4	2.4	1.7	2.0	3.6	10.9	3.5	2.9	3.8	2.3
n-C_{19}	16.2	30.4	3.8	2.9	0.5	2.8	1.8	1.9	11.0	3.1	3.2	2.6	3.5	2.5
n-C_{20}	17.0	34.0	5.3	3.2	0.5	2.9	1.7	1.7	11.0	3.0	2.9	2.5	4.1	0.7
n-C_{21}	11.4	25.8	4.5	4.0	0.5	3.0	1.7	2.1	9.3	2.8	3.0	2.4	3.0	1.8
n-C_{22}	24.4	29.0	5.4	3.4	0.5	2.7	1.7	1.9	10.3	3.1	3.6	2.9	3.8	1.7
n-C_{23}	19.0	21.5	5.6	3.9	0.6	2.7	1.5	2.0	9.9	2.9	3.3	2.7	3.1	1.4
n-C_{24}	25.6	17.6	8.8	3.9	0.3	2.5	1.2	2.0	7.7	2.0	2.4	2.0	2.1	1.0
n-C_{25}	24.0	23.4	7.3	5.8	0.5	3.8	1.2	2.4	9.5	2.0	1.4	1.4	1.2	0.7
n-C_{26}	47.7	11.2	7.7	3.3	0.3	1.9	0.5	1.2	4.3	1.0	0.7	0.6	0.5	0.3
n-C_{27}	35.0	2.0	6.1	5.7	1.2	3.6	0.8	2.0	16.6	2.4	1.3	1.2	0.8	0.8
n-C_{28}	41.4	10.4	12.3	3.2	0.3	2.1	0.4	1.1	4.3	0.8	0.4	0.3	0.2	0.2
n-C_{29}	29.5	64.1	7.2	13.6	0.9	7.6	1.3	5.6	33.0	3.9	2.1	1.8	1.1	1.3
n-C_{30}	79.4	15.4	12.1	3.6	0.3	2.6	0.5	1.3	5.7	0.8	0.7	0.4	0.2	0.4
n-C_{31}	40.8	64.7	7.3	9.5	0.6	5.7	1.3	3.3	30.1	4.0	2.6	2.2	1.5	1.6
n-C_{32}	20.0	16.7	9.7	3.7	0.3	2.5	0.6	1.2	6.2	0.9	0.9	0.5	0.2	0.4
n-C_{33}	39.1	63.4	7.7	6.2	0.4	3.7	0.8	2.1	24.0	2.0	1.9	1.2	0.6	0.8
n-C_{34}	49.4	14.7	7.8	4.1	0.2	2.8	0.5	1.6	4.7	0.6	0.7	0.3	0.1	0.4
n-C_{35}	39.6	24.2	0.8	3.9	0.1	2.4	<0.1	1.6	7.1	0.8	0.6	0.4	0.2	0.4
n-C_{36}	32.8	1.9	0.3	0.9	<0.1	1.1	0.2	0.6	2.8	0.2	0.4	0.1	<0.1	nd
n-C_{37}	1.4	1.9	nd	0.9	nd	0.8	<0.1	0.1	0.1	0.1	0.3	0.2	nd	nd
n-C_{38}	nd	nd	nd	0.3	nd	0.2	<0.1	0.1	2.2	nd	0.2	0.1	nd	nd
∑ *n*-alkanes	**659.6**	**587.3**	**128.5**	**95.8**	**9.3**	**65.2**	**24.0**	**42.2**	**246.5**	**48.0**	**43.7**	**35.2**	**38.1**	**23.8**
n-C_{17}/*Pr*[a]	0.8	0.4	0.8	0.7	0.7	0.7	0.5	0.6	0.7	0.5	0.5	0.6	0.6	0.5
n-C_{18}/*Phy*[b]	0.9	0.9	0.9	0.9	0.8	0.9	0.8	0.7	0.9	0.8	0.8	0.8	0.7	0.8
HMW[c]	577.5	442.1	115.8	83.1	7.6	54.5	16.0	34.1	198.9	33.2	29.3	23.3	22.7	13.7
n-C_{29}/*n*-C_{17}[d]	3.2	4.6	6.3	9.3	4.5	6.4	1.6	6.0	5.9	2.5	1.5	1.4	0.6	1.3
TAR[d]	3.6	2.9	4.0	6.5	3.9	4.2	1.2	3.9	4.8	2.2	1.3	1.3	0.7	1.0
TMD[e]	2.8	2.4	2.3	3.3	2.0	2.5	0.9	2.2	3.1	1.4	0.8	0.9	0.5	0.8

[a] Pristane.
[b] Phytane.
[c] HMW: high molecular weight calculated as *n*-alkanes with >20 carbon atoms.
[d] TAR: terrigenous/aquatic ratio calculated as ($nC_{27} + nC_{29} + nC_{31}$) / ($nC_{15} + nC_{17} + nC_{19}$) (Bourbonniere and Meyers, 2016).
[e] TMD: terrestrial-marine discriminant calculated as [∑ odd chains $n(C_{25} - C_{33})$ / ∑ odd chain $n(C_{15} - C_{23})$] (Syakti et al., 2012).

Table 4
Concentration of PAHs in sediment samples of emissary 1 and 2 (O1 and O2) and their respective class fractions (μg·kg^{-1} dw).

	O1	O2	O1A	O1B	O1C	O1D	O1E	O1F	O2A	O2B	O2C	O2D	O2E	O2F
Compound														
Na	dl	dl	dl	dl	dl	dl	dl	dl	dl	dl	dl	dl	dl	dl
Ace	dl	dl	dl	dl	dl	dl	dl	dl	dl	dl	dl	dl	dl	dl
Ac	2	1	dl	dl	dl	dl	dl	dl	dl	dl	dl	dl	dl	dl
Fr	9	2	4	1	dl	dl	2	2	3	3	2	2	2	2
Phe	365	72	119	122	44	43	0	24	7	30	18	2	1	5
Ant	216	73	99	35	30	40	2	9	9	15	12	2	2	4
Fl	648	436	59	208	106	115	11	88	178	89	60	12	9	13
Pyr	548	630	66	169	126	111	14	56	36	116	74	19	14	21
B[*a*]Ant	53	13	29	4	2	6	dl	dl	dl	dl	dl	dl	dl	dl
Chry	732	755	108	370	30	38	0	38	32	136	73	dl	dl	dl
B[*b*]Fl	dl	dl	dl	dl	dl	dl	dl	dl	dl	dl	dl	dl	dl	dl
B[*k*]Fl	746	900	57	52	148	209	dl	207	529	183	90	dl	dl	dl
B[*a*]Pyr	470	678	27	8	107	139	1	147	42	137	65	1	1	1
IPyr	125	74	56	dl	4	18	dl	36	4	35	1	dl	dl	dl
dB[*ah*]Ant	37	27	10	12	3	dl	dl	dl	dl	dl	dl	dl	dl	dl
B[*ghi*]P	122	114	19	16	dl	24	dl	35	13	35	10	dl	dl	dl
∑ PAH[a]	**4075**	**3779**	**653**	**998**	**601**	**744**	**30**	**643**	**854**	**775**	**406**	**39**	**29**	**47**
Molecular diagnostic														
Ant / (Ant + Phe)	0.4	0.1	1.2	3.5	1.5	1.1	0.2	2.6	0.8	2.0	1.5	1.1	0.6	1.2
BaA / (BaA + Chry)	0.5	0.7	0.9	1.2	0.8	1.0	0.7	1.6	4.9	0.8	0.8	0.6	0.6	0.6
IPyr / (IPyr + BghiP)	0.5	0.4	0.5	0.5	0.5	0.5	0.4	0.6	0.8	0.4	0.4	0.4	0.4	0.4
LMW / HMW[b]	0.2	~0	0.5	0.2	0.1	0.1	0.2	0.1	~0	0.1	0.1	0.2	0.2	0.3

[a] Sum of the 16 US EPA PAH.
[b] Sum of 2- and 3-ring PAHs divided by the sum of 4- to 6-ring PAHs.

of benzene rings (<4). Our finding supported that physicochemical characteristics such as Kow and Koc values may be responsible for settling distribution resemblance.

3.3. Sediment quality significance

Because many studies found that *n*-alkanes are not considerably toxic, the threshold value for *n*-alkanes has not yet been established. By comparing the results of several studies, we proposed in this study a value of 5000 ng/g for non-contaminated sediments, 5000–50,000 ng/g for urbanised sediments, and a value exceeding 50,000 ng/g for petroleum-contaminated sediments (Kanzari et al., 2012; Wagener et al., 2012; Syakti et al., 2012). Table 1 shows that the ∑ *n*-alkanes were 353 and 435.3 ng/g for O1 and O2, respectively. These values mean no immediate risk for the environment and living biota; however, it should be noted that our samples were discrete samples after flooding, and thus, we should focus on a sedimentary accumulation phenomenon on the downstream of the Cortiou channel outfall because the two last fractions represent 14–18% of both mass contributions of the transported particles and the ∑ *n*-alkanes-containing contaminants (O1E, O1F, O2E, O2F). As reported by Le Masson (1997), the treatment plant, one of the largest in Europe (1.8 million inhabitant eq.), has a flow of 7500 M^3 y^{-1}, while 17,000 M^3 y^{-1} has been flushed out from the river containing SPM, with an annual discharge ca. 3950 t, from which 850 t comes from rivers, highlighting the main contribution of the WWTP (Oursel et al., 2014).

Concerning PAHs, LMW such as Na, Ace, Ac, F, Phe, Ant are considered to be acutely toxic, but pose no carcinogenic risk to aquatic organisms, whereas HMW (e.g., Fl, Pyr, B[*a*]Ant, Chry) are more chronically embedded in the sediments, and some of them are potentially carcinogenic (Moore and Ramamoorthy, 1984). Uthe (1991) stated that the higher acute toxicity of LMW is enhanced by their high water solubility, whereas the lower acute toxicity of HMW reflects their low water solubility.

Ecotoxicological risk evaluation has been conducted using two widely used sediment quality guidelines, i.e., threshold effects level (TEL) and effects range-low (ERL) (Birch et al., 2012). The total bulk of PAHs results for Na, Ac, Ace, Fr, B(a)A and B(b)Fl were below their respective TEL values (30, 10, 10, 20, 70 and 70 ng/g, respectively); 100% of the concentrations of Fl and Phy were between 110 and 600 and 150–660 ng/g, respectively, while An and Chy were 100% of the upper ERL value (90 and 380 ng/g, respectively) (Table 6). When we evaluated their behaviour in individual compounds, we noted that most of the compounds were below their TEL values. The probable argument supporting this result was the homogeneity of the particle distribution among the different fraction sizes. Several compounds occurred with high concentrations (Fl and B(k)F); their ERL values were reached or were in between their TEL and ERL values, indicating that flooding particles might have a potential toxicity with probable adverse effects. For PCBs, the value of TEL was 22 ng/g, and the ERL value has been replaced by the term probable effect level (PEL) (189 ng·g) (Long and MacDonald, 2006). When PCBs were analysed as a bulk O1 and O2 deposit, they showed values between TEL and PEL, indicating a source of medium potential risk apportionment for marine sedimentary biota. Fortunately, regarding the 5 and 6 classes of both O1 and O2, the transported particles might contribute little to the marine environment

Table 5
Concentration of PCBs in sediment samples of emissary 1 and 2 (O1 and O2) and their respective class fractions (μg·kg^{-1} dw).

Compound	O1	O2	O1A	O1B	O1C	O1D	O1E	O1F	O2A	O2B	O2C	O2D	O2E	O2F
CB-52	15.9	0.0	0.0	0.0	0.0	0.0	0.0	0.0	0.0	0.0	0.0	0.0	0.0	0.0
CB-101	**30.4**	8.6	15.6	2.3	0.0	8.7	14.4	16.5	6.1	3.1	0.0	0.0	0.0	0.0
CB-118	**33.9**	**28.7**	7.1	3.3	0.0	0.0	0.0	0.0	1.5	3.0	0.0	0.0	0.0	0.0
CB-138	**29.2**	**34.6**	5.7	5.9	0.0	0.0	0.0	0.0	11.8	6.0	0.0	2.2	0.0	0.0
CB-153	12.8	**29.3**	9.6	4.0	0.0	0.0	0.0	0.0	9.0	3.8	0.0	0.0	0.0	0.0
CB-180	11.0	0.0	15.4	1.5	0.0	0.0	0.0	0.0	0.0	0.0	0.0	0.0	0.0	0.0
∑ PBSc	133.2	101.1	**53.5**	17.0	0.0	8.7	14.4	16.5	**28.4**	15.9	0.0	2.2	0.0	0.0

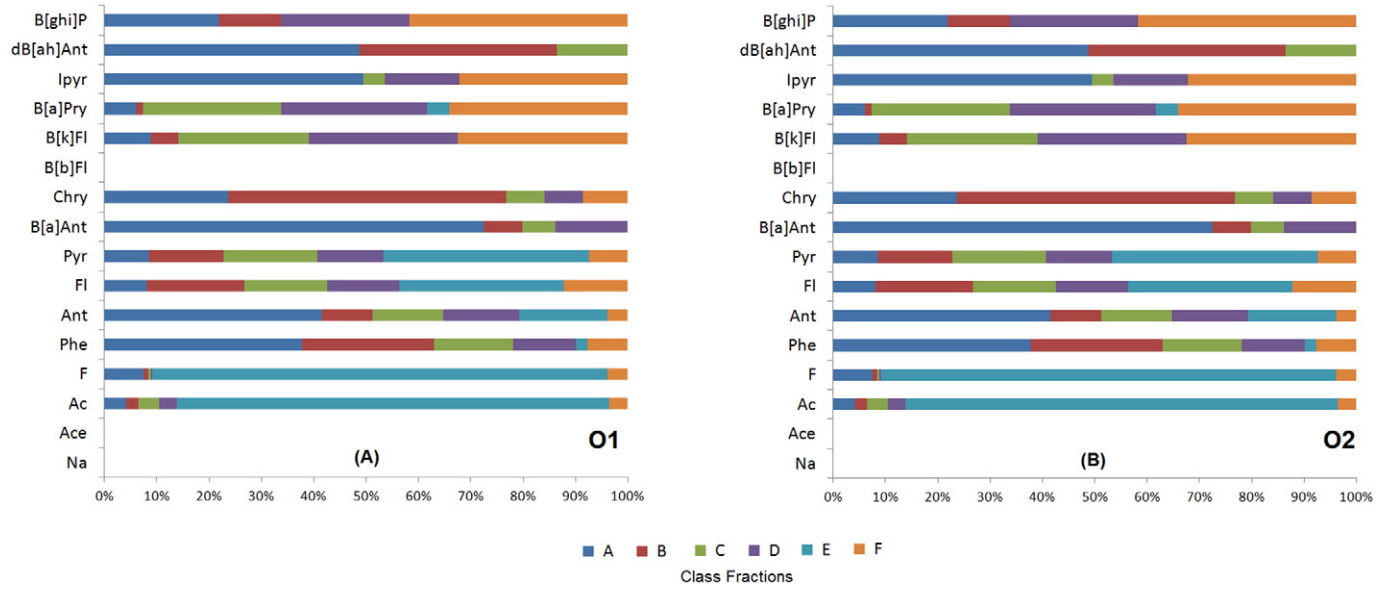

Fig. 5. Percentage of individuals PAH within each class fraction from emissary 1 and 2 (O1; Fig. 5A and O2; Fig. 5B).

because their respective values were far below the TEL threshold level (23 ng·g).

Concerning the extent of PCBs, the comparison with the international SQGs showed a moderate ecotoxicological risk (between TEL and ERL) for total O1 and O2. Nevertheless, the concentrations of some congeners (shown in **bold**) such as CB-101, CB-118 and CB-138 for O1 and CB-118, CB-138 and CB-158 for O2 were already higher than the threshold value (22 $\mu g \cdot kg^{-1}$ dw).

4. Conclusions

An experimental study was conducted to address the characteristic of urban run-off particles, which transport organic contaminants from two outlet channels of Geolide WWTP in Marseille. By conducting the settling velocity experiment, it was possible to determine the groups of fractions that are responsible for the contaminant enrichment in the marine environment. The median settling velocity was ca. 96.9 $\mu m\ s^{-1}$ for particle sizes ranging from 0.05 to 276.6 μm with a median size ca. 10.7 μm. The settling velocities exhibit a large variation among the classes that decrease with decreasing particle size and reduce the velocities on average by 40% for each subsequent class comparison. Through this study, we obtained evidence that multicontaminants (i.e. *n*-alkanes, PAHs and PCBs) were carried from the riverine and urban upstream with different maximum magnitudes. Through the settling velocity experiment, the determination of their characteristics and behaviours raises the new question regarding the use of different grain size in describing contaminants; this is because from certain fraction classes, we noted a contaminant profile with a predominance of the even carbon number preference of the n-C_{14} to n-C_{20}, which may be sourced from aquatic organisms (river, lake, and marine) or petroleum contamination. Integrated with *n*-alkanes, UCM, and low content Phe in PAHs, class fraction E was mainly derived from petroleum contamination. It is suggested that such petroleum molecular signatures were observed in SPM with particle size between 0.1 and 10 μm. From the perspective of environmental management, we need to gather more reliable and comprehensive data to provide an appropriate model of the contaminant flux and dispersion from the Cortiou outlet toward the marine environment, which is in the centre of the Calanque National Park that was recently established in 2012.

Table 6
Comparison of sediment quality guidelines of *n*-alkanes, PAH and PCB concentrations in different classes fraction of deposit settling particles from wastewater treatment emissaries (O1 and O2).

SQG TEL-ERL ($\mu g \cdot kg^{-1}$ dw)		% of occurrence		
		<TEL	TEL-ERL	>ERL
Na	30–160	100	–	–
Ace	10–20	100	–	–
Ac	10–40	100	–	–
Fr	20–20	100	–	–
Phe	90–240	79	14	7
Ant	50–90	72	14	14
Fl	110–600	64	29	7
Pyr	150–660	57	43	–
B[*a*]A	70–260	100	–	–
Chry	110–380	72	14	14
B[*b*]Fl	70–320	100	–	–
B[*k*]Fl	60–280	43	36	21
IPyr	–	–	–	–
dB[*ah*]Ant	–	–	–	–
B[*ghi*]P	–	–	–	–
∑PAHs	870–3500	25	56	19
∑PCBs (ICES)	22–189	–	100	–

Acknowledgement

The authors gratefully acknowledge the assistance of PROTEE laboratory from where Master's students participated in the sampling campaigns. This collaborative work was financially supported by the "ANR CES MARSECO (ANR-CESA-018-06).". Dr. Syakti, A.D acknowledges travel grant from DIPA UNSOED (DIPA/023.04.2.189899/2014). Constructive reviews by anonymous referees greatly improved the manuscript.

References

Ammann, A.A., Rüttimann, T.B., Bürgi, F., 2000. Simultaneous determination of TOC and TNb in surface and wastewater by optimised high temperature catalytic combustion. Water Res. 34 (14), 3573–3579.

Barakat, A.O., Kim, M., Qian, Y., Wade, T.L., 2002. Organochlorine pesticides and PCB residues in sediments of Alexandria Harbour, Egypt. Mar. Pollut. Bull. 44, 1421–1434.

Birch, H., Mayer, P., Lutzhøft, H.H.-C., Mikkelsen, P.S., 2012. Partitioning of fluoranthene between free and bound forms in stormwater runoff and other urban discharges using passive dosing. Water Res. 46, 6002–6012.

Bourbonniere, R.A., Meyers, P.A., 1996. Sedimentary geolipid records of historical changes in the watersheds and productivities of Lakes Ontario and Erie. Limnol. Oceanogr. 41, 352–359.
Callahan, J., Dai, M., Chen, R.F., Li, X., Lu, Z., Huang, W., 2004. Distribution of dissolved organic matter in the Pearl River Estuary, China. Mar. Chem. 89 (1–4), 211–224.
Commendatore, M.G., Nievas, M.L., Amin, O., Esteves, J.L., 2012. Sources and distribution of aliphatic and polyaromatic hydrocarbons in coastal sediments from the Ushuaia Bay (Tierra del Fuego, Patagonia, Argentina). Mar. Environ. Res. 74, 20–31.
de Souza, D.B., Machado, K.S., Froehner, S., Scapulatempo, C.F., Bleninger, T., 2011. Distribution of n-alkanes in lacustrine sediments from subtropical lake in Brazil. Chem. Erde 71, 171–176.
Fugate, D., Chant, B., 2006. Aggregate settling velocity of combined sewage overflow. Mar. Pollut. Bull. 52, 427–432.
Geptner, A.R., Richter, B., Pikovskii, Y.I., Chernyansky, S.S., Alekseeva, T.A., 2006. Hydrothermal polycyclic aromatic hydrocarbons in marine and lagoon sediments at the intersection between Tjörnes Fracture Zone and recent rift zone (Skjálfandi and Öxarfjörður bays), Iceland. Mar. Chem. 101 (3–4), 153–165.
Geyer, W.R., Hill, P.S., Kineke, G.C., 2004. The transport, transformation and dispersal of sediment by buoyant coastal flows. Estuar. Coast. Shelf Sci. 24, 927–949.
Grimalt, J., Albaiges, J., 1987. Sources and occurrence of C_{12}–C_{22} n-alkane distributionswith even carbon-number preference in sedimentary environments. Geochim. Cosmochim. Acta 51, 1379–1384.
Jany, C., Cossa, D., Djelalli, Z., Garnier, C., Mounier, S., Pairaud, I., Sauzade, D., Thouvenin, B., Zebracki, M., 2012. METROC: evaluation des apports de contaminants chimiques de la métropole marseillaise au milieu marin. Rapport Ifremer RST.ODE/LER/PAC/12–02 – Agence de l'eau AERM&C (140 pp.).
Jeng, W.-L., Chen, M.P., 1995. Grain size effect on bound lipids in sediments off northeastern Taiwan. Org. Geochem. 23 (4), 301–310.
Kanzari, F., Syakti, A.D., Asia, L., Malleret, L., Mille, G., Jamoussi, B., Abderrabba, M., Doumenq, P., 2012. Aliphatic hydrocarbons, polycyclic aromatic hydrocarbons, polychlorinated biphenyls, organochlorine, and organophosphorous pesticides in surface sediments from the Arc river and the Berre lagoon, France. Environ. Sci. Pollut. Res. 19 (2), 559–576.
Kanzari, F., Syakti, A.D., Asia, L., Malleret, L., Piram, A., Mille, G., Doumenq, P., 2014. Distributions and sources of persistent organic pollutants (aliphatic hydrocarbons, PAHs, PCBs and pesticides) in surface sediments of an industrialized urban river (Huveaune), France. Sci. Total Environ. 478, 141–151.
León, V.M., García, I., Martínez-Gómez, C., Campillo, J.A., Benedicto, J., 2014. Heterogeneous distribution of polycyclic aromatic hydrocarbons in surface sediments and red mullet along the Spanish Mediterranean coast. Mar. Pollut. Bull. 87, 352–363.
Long, E.R., MacDonald, D.D., 2006. Calculation and uses of mean sediment quality guidelines quotients: a critical review. Sci. Environ. Sci. Technol. 40, 1726–1736.
Lorrain, A., Savoye, N., Chauvaud, L., Paulet, Y.-M., Naulet, N., 2003. Decarbonation and preservation method for the analysis of organic C and N contents and stable isotope ratios of low-carbonated suspended particulate material. Anal. Chim. Acta 491, 125–133.
Mantovanelli, A., Ridd, P.V., 2006. Device to measure settling velocities of cohesive sediment aggregates: a review of the in situ technology. J. Sea Res. 56, 199–226.
Mazzella, N., Molinet, J., Syakti, A.D., Bertrand, J.C., Doumenq, P., 2007. Assessment of the effects of hydrocarbon contamination on the sedimentary bacterial communities and determination of the polar lipid fraction purity: relevance of intact phospholipid analysis. Mar. Chem. 103 (3–4), 304–317.
Mille, G., Asia, L., Guiliano, M., Malleret, L., Doumenq, P., 2007. Hydrocarbons in coastal sediments from the Mediterranean Sea (Gulf of Fos area, France). Mar. Pollut. Bull. 54, 566–575.
Moore, J.W., Ramamoorthy, S., 1984. Aromatic hydrocarbons: polycyclics. In: DeSanto, R.S. (Ed.), Organic Chemicals in Natural Waters: Applied Monitoring and Impact Assessment. Springer– Verlag, New York.
Neşer, G., Kontas, A., Ünsalan, D., Altay, O., Darılmaz, E., Uluturhan, E., Küçüksezgin, F., Tekoğul, N., Yercan, F., 2012. Polycyclic aromatic and aliphatic hydrocarbons pollution at the coast of Aliağa (Turkey) ship recycling zone. Mar. Pollut. Bull. 64 (5), 1055–1059.
Oursel, B., Garnier, C., Pairaud, I., Omanovic, D., Durrieu, G., Syakti, A.D., Le Poupon, C., Thouvenin, B., Lucas, Y., 2014. Behaviour and fate of urban particles in coastal waters: settling rate, size distribution and metals contamination characterization. Estuar. Coast. Shelf Sci. 138, 14–26.
Papenmeier, S., Schrottke, K., Bartholoma, A., 2014. Over time and space changing characteristics of estuarine suspended particles in the German Weser and Elbe estuaries. J. Sea Res. 85, 104–115.
Patrolecco, L., Ademollo, N., Capri, S., Pagnotta, R., Polesello, S., 2010. Occurrence of priority hazardous PAHs in water, suspended particulate matter, sediment and common eels (*Anguilla anguilla*) in the urban stretch of the River Tiber (Italy). Chemosphere 81, 1386–1392.
Perianez, R., 2005. Modelling the transport of suspended particulate matter by the Rhone River plume (France). Implication for pollutant dispersion. Environ. Pollut. 133, 351–364.
Sanderson, E.G., Raqbi, A., Vyskocil, A., Farant, J.-P., 2004. Comparison of particulate polycyclic aromatic hydrocarbon profiles in different regions of Canada. Atmos. Environ. 38, 3417–3429.
Syakti, A.D., Asia, L., Kanzari, F., Umasangadji, H., Malleret, L., Mille, G., Doumenq, P., 2012. Distribution of organochlorine pesticides (OCs) and polychlorinated biphenyls (PCBs) in marine sediments directly exposed to wastewater sewer outfall of Cortiou, Marseille. Environ. Sci. Pollut. Res. 19 (5), 1524–1535.
Tian, Y.-Z., Li, W.-H., Shi, G.-L., Feng, Y.-C., Wang, Y.-Q., 2013. Relationships between PAHs and PCBs, and quantitative source apportionment of PAHs toxicity in sediments from Fenhe reservoir and watershed. J. Hazard. Mater. 248–249, 89–96.
Uthe, J.F., 1991. Polycyclic aromatic hydrocarbons in the environment. Can. Chem. News 43 (7) (25–2).
Vystavna, Y., Huneau, F., Schäfer, J., Motelica-Heino, M., Blanc, G., Larrose, A., Vergeles, Y., Dyadin, D., Le Coustumer, P., 2012. Distribution of trace elements in waters and sediments of the Seversky Donets transboundary watershed (Kharkiv Region, Eastern Ukraine). Appl. Geochem. 27, 2077–2087.
Wafo, E., Sarrazin, L., Diana, C., Schembri, T., Lagadec, V., Monod, J.L., 2006. Polychlorinated biphenyls and DDT residues distribution in sediments of Cortiou (Marseille, France). Mar. Pollut. Bull. 52, 104–107.
Wagener, A.L.R., Meniconi, M.F.G., Hamacher, C., Farias, C.O., da Silva, G.C., Gabardo, I.T., Scofield, A.L., 2012. Hydrocarbons in sediments of a chronically contaminated bay: the challenge of source assignment. Mar. Pollut. Bull. 64, 284–294.
Wang, X.C., Sun, S., Ma, H.Q., Liu, Y., 2006. Sources and distribution of aliphatic and polyaromatic hydrocarbons in sediments of Jiaozhou Bay, Qingdao, China. Mar. Pollut. Bull. 52, 129–138.
Wang, Y., Fang, X., Zhang, T., Li, Y., Wu, Y., He, D., Wang, H., 2010. Predominance of even carbon-numbered n-1 alkanes from Lacustrine sediments in Linxia Basin, NE Tibetan Plateau: implications for climate change. Appl. Geochem. 25 (10), 1478–1486.
Winterwerp, J.C., 2002. On the flocculation and settling velocity of estuarine mud. Cont. Shelf Res. 22, 1339–1360.
Yunker, M.B., Macdonald, R.W., Vingarzan, R., Mitchell, R.H., Goyette, D., Sylvestre, S., 2002. PAHs in the Fraser River basin: a critical appraisal of PAH ratios indicators of PAH source and composition. Org. Geochem. 33, 489–515.
Zhang, W., Wei, C., Chai, X., He, J., Cai, Y., Ren, M., Yan, B., Peng, P., Fu, J., 2012. The behaviours and fate of polycyclic aromatic hydrocarbons (PAHs) in a coking wastewater treatment plant. Chemosphere 88, 174–182.
Zhou, J.L., Fileman, T.W., Evans, S., Donkin, P., Llewellyn, C., Readman, J.W., Mantoura, R.F.C., Rowland, S.J., 1998. Fluoranthene and pyrene in the suspended particulate matter and surface sediments of the Humber Estuary, UK. Mar. Pollut. Bull. 36 (8), 587–597.